

## Model of room-temperature resonant-tunneling current in metal/insulator and insulator/insulator heterostructures

C. Strahberger\* and P. Vogl†

Walter Schottky Institut and Physik Department, Technische Universität München, 85748 Garching, Germany

(Received 16 February 2000)

Employing a multiband scattering formalism for ballistic tunneling currents, a systematic theoretical study of the current-voltage characteristics of metal-insulator and insulator-based resonant-tunneling diodes is presented. We predict ultrathin metal( $\text{CoSi}_2$ )/insulator( $\text{CaF}_2$ ) and insulator( $\text{CdF}_2$ )/insulator( $\text{CaF}_2$ ) heterostructures on silicon substrates to be excellent candidates for room-temperature quantum-effect devices. The scattering formalism in the framework of tight-binding theory is cast in a particularly compact and transparent form that is applicable to long-range tight-binding interactions and complex unit cells. The results are in good agreement with experimental data. The physical origin of the distinct current resonances, particularly in the metal/insulator structures, is explained in detail and found to originate in the localized character of the transition-metal  $d$  states. Furthermore, the stability of the resonance characteristics with regard to layer thickness variations, substrate orientations, and interface roughness is predicted.

### I. INTRODUCTION

Silicon-compatible quantum-effect devices that have the potential to operate at room temperature are of considerable relevance to semiconductor research. Promising candidates that have recently attracted attention are heterostructures consisting of metallic  $\text{CoSi}_2$  and insulating  $\text{CaF}_2$  or  $\text{CdF}_2$  layers. These fluorite structure materials can be grown pseudomorphically on top of each other<sup>1,2</sup> as well as on silicon substrate of various orientations.<sup>3</sup> Particularly, the heterostructure bandoffsets of the  $\text{CoSi}_2/\text{CaF}_2$ ,  $\text{CdF}_2/\text{CaF}_2$ , and  $\text{CaF}_2/\text{Si}$  interfaces are sufficiently large to provide quantum confinement at room temperature. Recently, it was shown that resonant tunneling diodes (RTD) can be successfully fabricated with these materials.<sup>4-7</sup> In contrast to standard semiconductor RTD's,<sup>8,14,15,11</sup> however, very few detailed theoretical studies have been performed for these types of metal-insulator RTD's so far.<sup>16</sup>

In this paper, we predict that double and triple barrier resonant-tunneling diodes based on  $\text{CoSi}_2/\text{CaF}_2$  and  $\text{CdF}_2/\text{CaF}_2$  heterostructures can lead to distinct current peaks with a high peak-to-valley ratio at room temperature. We show that the metallic and insulating heterostructures lead to sharp current resonances that originate in the detailed electronic structure of the constituent materials. The present theory illustrates the physics of these resonances and predicts the influence of key parameters such as well and barrier widths or interface roughness on the current-voltage characteristics.

Here the standard Landauer-Büttiker formalism for the ballistic tunneling current is employed.<sup>20-22</sup> The transmission matrix is determined in terms of the extended transfer-matrix method within the tight-binding framework.<sup>9-14,17-19</sup> We present a compact and concise formulation of this technique including several numerical improvements, which makes it particularly suitable for complex metal/insulator structures.

The paper is organized as follows: In Sec. II we briefly describe the theory and numerical implementation of the calculations. Section III discusses the electronic structure of the metallic and insulating materials that form the RTD's, with

emphasis on the interface properties. In Sec. IV we present results for a RTD's involving  $\text{CoSi}_2/\text{CaF}_2$  heterostructures and compare them to available experiments. In Sec. V double and triple barrier  $\text{CdF}_2/\text{CaF}_2$  heterostructures are discussed. Finally, the paper is concluded in Sec. VI.

### II. MODEL

This paper focuses on ultrathin nm-scale tunneling structures consisting of metallic and insulating layers.<sup>16</sup> We assume these structures to be sufficiently thin that the coherent contribution to the tunneling current dominates so that the incoherent parts can be neglected. In order to adequately model the complex electronic structure of the constituent materials, a multiband, multichannel transfer-matrix-type of approach within the empirical tight-binding theory<sup>23</sup> is used. Early variants of the transfer-matrix method were developed in Refs. 9-12. Later refinements made it possible to compute large structures up to micrometer length.<sup>12-14</sup> In materials with large unit cells, however, transfer matrices often become singular rendering the standard approach inapplicable. A proper generalization of the method that allows the calculation of currents for arbitrary structures has been developed by Boykin.<sup>17,18</sup> Analytical approximations of the transmission coefficient have been developed by Bowen *et al.*<sup>19</sup>

#### A. Complex band structure

To set up the notation and briefly review the basic calculational procedure, consider a thin pseudomorphically grown heterostructure along the  $z$  direction that is sandwiched in between two semi-infinite bulk contacts (that may be different). The Bloch states of these contacts are the *in* and *out* states of the scattering problem and are characterized by the reservoir (L for left and R for right), the energy  $E$ , and the lateral wave vector  $\mathbf{k}_\parallel$  that are conserved during this ballistic scattering process, and the wave vector  $k_z$  along the growth axis. By solving the Schrödinger equation of the whole device with scattering boundary conditions,<sup>14,17,18</sup> one can cal-

culate the transmission probability  $T$  for an *in*-propagating Bloch state from the left contact to tunnel into any *out*-propagating state of the right contact. It is convenient to vertically subdivide the whole device into slices that consist of a few atomic layers. They can be chosen in such a way that tight-binding matrix elements are nonzero only between neighboring slices and one lattice vector lies along the  $z$  direction and is perpendicular to the other two. We enumerate the slices within the heterostructure by  $s=1, \dots, N$ . The slices that lie completely within the left (right) bulk are labeled by  $s \leq 0$  ( $s > N$ ). The tight-binding basis that is used to represent all scattering states is the set of two-dimensional Bloch states that are characterized by  $\mathbf{k}_{\parallel}$ , the basis orbitals within the lateral unit cell in a given slice, and the slice index  $s$ . By expanding the wave function of the left bulk in terms of these basis states, its coefficients  $\mathbf{C}_s$  obey the Schrödinger equation in the form of

$$(H_{intra} - E)\mathbf{C}_s + H_{inter}\mathbf{C}_{s-1} + H_{inter}^{\dagger}\mathbf{C}_{s+1} = 0, \quad (1)$$

together with the Bloch condition

$$\mathbf{C}_s = e^{ik_z d_z} \mathbf{C}_{s-1}, \quad (2)$$

where  $s < 0$  and  $H_{intra}$  and  $H_{inter}$  are the intra- and interslice bulk Hamiltonian matrices for the left bulk. Note that the dimension  $M$  of the vector  $\mathbf{C}_s$  is determined by the number of orbitals within the lateral unit cell and  $d_z$  is the length of the slices in the left bulk. Analogous equations hold for the right bulk. Equations (1) and (2) can only be converted into an eigenvalue equation for  $k_z$  if  $H_{inter}$  is an invertible matrix. As pointed out recently,<sup>17,18</sup> however, this is almost never the case for realistic tight-binding models. Nevertheless, one can transform Eqs. (1) and (2) into a generalized eigenvalue equation of dimension  $2M \times 2M$  that does not involve the inverse of  $H_{inter}$ ,<sup>17,18</sup>

$$\begin{pmatrix} (H_{intra} - E) & H_{inter}^{\dagger} \\ 1 & 0 \end{pmatrix} \begin{pmatrix} \mathbf{C}_s \\ \mathbf{C}_{s+1} \end{pmatrix} = \lambda \begin{pmatrix} -H_{inter} & 0 \\ 0 & 1 \end{pmatrix} \begin{pmatrix} \mathbf{C}_s \\ \mathbf{C}_{s+1} \end{pmatrix} \quad (3)$$

where  $\lambda = e^{-ik_z d_L}$  with  $2M$  complex solutions  $k_z$  that correspond to the left bulk. These  $2M$  solutions are linearly independent since the kernels of both matrices in Eq. (3) have no nonzero element in common as one can easily show.

### B. Scattering formalism

Based on this scheme of the complex band structure, we now calculate the transmission coefficient in a particularly compact and transparent form. This method generalizes the approach of Refs. 14 and 18 to situations where the right and left contact materials are different. This requires a careful normalization of the asymptotic scattering states.

The first step consists in calculating the group velocity  $v_z$  normal to the slice for each bulk. The latter allows one to classify the  $2M$  solutions of Eq. (3) into  $M$  bulk solutions that propagate ( $v_z \geq 0$  if  $\text{Im} k_z = 0$ ) or decay ( $\text{Im} k_z \geq 0$ ) to the right and the remaining  $M$  bulk states that propagate or decay to the left. Since the eigenvectors of Eq. (3) occur in pairs  $(k_z, -k_z)$  this splitting into two parts of equal size is always possible. We will denote the first type of states by  $k_z^{\rightarrow}$

and the opposite by  $k_z^{\leftarrow}$ , respectively. We now order these bulk eigenvectors, normalized to  $1/\sqrt{2d_z}$ , columnwise such that the first  $M$  eigenvectors correspond to the states  $|L, k_z^{\rightarrow}\rangle$ , whereas the remaining  $M$  columns are the states  $|L, k_z^{\leftarrow}\rangle$ . For each of these 2 types of states, the propagating states are arranged before the evanescent ones. In this way, a  $2M \times 2M$  eigenvector matrix  $\mathcal{C}$  is formed. The normalization guarantees current conservation in the case where the slices in the left and right reservoir have different widths.

We discuss the procedure only for the left bulk; the right bulk solutions are treated analogously. The key point is that the inverse  $\mathcal{C}^{-1}$  acts as a projector onto any scattering wave function of the device and decomposes its components into states propagating (or decaying) to the right and to the left,

$$\begin{pmatrix} \langle L, k_z^{\rightarrow} | \psi \rangle \\ \langle L, k_z^{\leftarrow} | \psi \rangle \end{pmatrix} = \mathcal{C}^{-1} | \psi \rangle = \begin{pmatrix} D_{\rightarrow} \\ D_{\leftarrow} \end{pmatrix} | \psi \rangle, \quad (4)$$

which follows from  $\mathbf{1} = \mathcal{C}^{-1}\mathcal{C}$  or  $\mathbf{1}_{k_j} = \mathcal{C}^{-1}\mathbf{C}_{k_j}$  in component form for the  $k_j$ th eigenvector. Correspondingly,  $\mathcal{C}^{-1}$  has been decomposed into its upper- and lower-half, which defines the  $M \times 2M$  matrices  $D_{\rightarrow}$  and  $D_{\leftarrow}$ , respectively.

The scattering problem for the total device that properly incorporates the boundary conditions can now be written in the form

$$\begin{pmatrix} D_{\rightarrow}^L 0 \dots 0 \\ H_{device} - E\mathbf{1} \\ 0 \dots 0 D_{\leftarrow}^R \end{pmatrix} \begin{pmatrix} \mathbf{C}_{-1} \\ \mathbf{C}_0 \\ \vdots \\ \mathbf{C}_{N+1} \\ \mathbf{C}_{N+2} \end{pmatrix} = \begin{pmatrix} \mathbf{I}_{k_z} \\ \mathbf{0} \\ \mathbf{0} \end{pmatrix}. \quad (5)$$

Here,  $H_{device}(\mathbf{k}_{\parallel})$  is the Hamiltonian matrix inside the device including the coupling to the first bulk slice at each contact and  $E$  is the given energy. The vector  $\mathbf{I}_{k_z}$  is a unit vector of dimension  $M$  that contains its only nonzero element in a row that corresponds to the propagating Bloch state  $k_z^{\rightarrow}$ . The zeros in the last row of the vector on the right-hand side guarantee that the solution contains no  $|R, k_z^{\leftarrow}\rangle$  states. In addition, the zeros in  $\mathbf{I}_{k_z}$  exclude states of the left bulk that decay exponentially towards the heterostructure. Equation (5) must be solved for each propagating bulk state  $|L, k_z^{\rightarrow}\rangle$ . The transmitted amplitude coefficients can be written in the following compact form,

$$t(E, \mathbf{k}_{\parallel}, k_z^{\rightarrow}) = (D_{\rightarrow}^R) \begin{pmatrix} \mathbf{C}_{N+1} \\ \mathbf{C}_{N+2} \end{pmatrix}. \quad (6)$$

Finally, the probability current from the  $i$ th incoming Bloch state  $k_{z,i}^{\rightarrow}$  to the  $j$ th outgoing Bloch state  $k_{z,j}^{\leftarrow}$  is obtained by weighing the square of the corresponding amplitude ratios with the normal group velocity ratio of the outgoing and incoming wave,

$$T(E, \mathbf{k}_{\parallel}, k_{z,i}^{\rightarrow} \rightarrow k_{z,j}^{\leftarrow}) = |t(E, \mathbf{k}_{\parallel}, k_{z,i}^{\rightarrow} \rightarrow k_{z,j}^{\leftarrow})|^2 \frac{v_{z,j}^R}{v_{z,i}^L}. \quad (7)$$

By summing this transmission probability over all possible *in* and *out* states  $k_z$  and integrating it over energy and lateral wave vector, weighted with the Fermi distribution functions, one finally obtains the current.<sup>22</sup> For the evaluation Eq. (7), the group velocity component in growth direction must be computed frequently. The formalism outlined above allows one to compute it very efficiently as a by-product in terms of the bulk quantities  $\mathbf{C}_0$  and  $H_{inter}$  in Eq. (3),

$$v_z^L(E, \mathbf{k}_{\parallel}, k_z^{\rightarrow}) = -\frac{2d_z}{\hbar|\mathbf{C}_0|^2} \text{Im}(\mathbf{C}_0^\dagger H_{inter} \mathbf{C}_0 e^{ik_z^{\rightarrow} d_z}), \quad (8)$$

which follows from the Hellman-Feynman theorem.

### C. Numerical details

Due to the complex band structure of the metallic CoSi<sub>2</sub>, the calculated transmission coefficients shows many sharp peaks over the whole energy range and wave-vector-space. It requires some care to properly integrate these tunneling ‘‘hot spots.’’ Therefore, the three-dimensional  $(E, \mathbf{k}_{\parallel})$  integration in the Landauer-Büttiker expression for the current density has been performed with an adaptive integration scheme. For the lateral momentum integration, the irreducible wedge of the projected Brillouin zone is first covered by a square grid. Subsequently, the mesh is tightened recursively around the highly transmitting regions. In each of these refining steps, grid points are added locally in such a way that the grid alternates between simple square and face centered to ensure that all previously included lattice points are taken into account. This efficient procedure is typically equivalent to 230 000 integration points on a fixed grid.

### III. BAND STRUCTURE AND BAND OFFSETS

We consider heterostructures consisting of the compounds CoSi<sub>2</sub>, CaF<sub>2</sub>, and CdF<sub>2</sub>. All of them possess the same cubic fluorite ( $O_h^F$ ) crystal structure. Furthermore, they are Si compatible in the sense that they can be grown pseudomorphically on Si(111) substrates with very small lattice mismatch; their lattice constants are given by 5.356 Å, 5.462 Å, and 5.388 Å, respectively. The precise atomic positions at the interface are well established for CaF<sub>2</sub>/Si,<sup>24,25</sup> but less so for CoSi<sub>2</sub>/CaF<sub>2</sub> and CdF<sub>2</sub>/CaF<sub>2</sub>.

The symmetry in the case of stoichiometric growth of CoSi<sub>2</sub> on CaF<sub>2</sub> as well as total energy calculations<sup>26</sup> suggest the interface layer of CoSi<sub>2</sub>/CaF<sub>2</sub> to contain Si and F, which implies that the layer sequence along [111] consists of complete Si-Co-Si and F-Ca-F triple layers. In addition, CoSi<sub>2</sub> on the CaF<sub>2</sub> substrate can have 2 plausible orientations: either the lattice is continued across the interface (type A) or the crystal structure of CoSi<sub>2</sub> is rotated by 180° in the growth direction with respect to the underlying substrate (type B). Several experiments<sup>27,28</sup> indicate that the CoSi<sub>2</sub>/CaF<sub>2</sub> interface possess a type-B orientation. Therefore we have assumed a type-B interface throughout. In addition, there is another degree of freedom, i.e., three possible types of layer stackings above the interface. Only one of them fits all bulk distances closely. Table I gives this optimum type-B stacking sequence along the [111] direction. We have increased the

TABLE I. Layer sequences (stacking) near the (111)-CaF<sub>2</sub>/CoSi<sub>2</sub> interface as assumed in the present calculations and in previous work.

| CoSi <sub>2</sub> /CaF <sub>2</sub> |        | Si | Co | Si | F | Ca | F |
|-------------------------------------|--------|----|----|----|---|----|---|
| This paper                          | type B | C  | A  | B  | A | C  | B |
| Akai <i>et al.</i> <sup>a</sup>     | type A | C  | A  | B  | A | B  | C |

<sup>a</sup>Reference 26.

Si-F interface distance slightly in such a way that the Ca-Si distance across the interface equals its bulk value of 3.1 Å. We note that recent total-energy calculations<sup>26</sup> assumed an unrelaxed type-A interface, which implies an extremely compressed Ca-Si distance of only 2.3 Å.

A type-A interface is much more plausible for the CaF<sub>2</sub>/CdF<sub>2</sub> interface since both solids have quite similar properties. Thus, we have assumed a perfect continuation of the fluorite lattice across the interface even though other orientations have also been observed in some samples.<sup>29</sup>

Optimized empirical tight-binding (TB) parameters enable us to obtain numerically efficient and realistic band structures. In addition to that the effects of elastic strain were incorporated into the calculation by scaling the so-called hopping matrix elements according to the universal law found by Harrison.<sup>30,31</sup> Since at the various interfaces these hopping matrix elements are unknown, universal couplings<sup>32</sup> were adapted to the measured or expected interface geometry.<sup>24,25</sup> The local electrostatic potential  $\Phi(\mathbf{r})$  as well as experimental band offsets have been incorporated by the substitution of the orbital ‘‘on-site’’ energies:<sup>33</sup>

$$E_\alpha \rightarrow E_\alpha - e\Phi(\mathbf{r}). \quad (9)$$

The tight-binding parameters for CoSi<sub>2</sub> and for the contact materials Si and Al were taken from Refs. 34, 35, and 36, respectively. For CaF<sub>2</sub>, we have developed a  $sp^3s^*$ -TB model by fitting the band structure at high-symmetry points both to first-principles results<sup>37</sup> and experiments.<sup>38</sup> For CdF<sub>2</sub>, a model with a single *s* band proved sufficient to fit the known conduction-band data.<sup>39</sup> Table II lists the resulting nearest neighbor TB parameters.

The TB parameters need to be augmented by band offsets to align the band structures with respect to one another. In Table III we compare experimental and previously obtained theoretical band offsets. For the Si/CaF<sub>2</sub> interface as well as for the CaF<sub>2</sub>/CdF<sub>2</sub> interface these results are seen to be con-

TABLE II. The nearest-neighbor tight-binding parameters for bulk CaF<sub>2</sub> and CdF<sub>2</sub> in eV. The conventional notation for the matrix elements in the two-center approximation is used (Ref. 35).

|                  | $ss\sigma$ | $sp\sigma$ | $ps\sigma$ | $pp\sigma$ | $pp\pi$ | $ss^*\sigma$ |
|------------------|------------|------------|------------|------------|---------|--------------|
| Ca-F             | -1.139     | 0.360      | 1.086      | 3.776      | -0.088  | 0.604        |
| Cd-F             | -2.6178    |            |            |            |         |              |
|                  |            | $E(s)$     | $E(p)$     | $E(s^*)$   |         |              |
|                  | Ca         | 5.75       | 10.4       |            |         |              |
| CaF <sub>2</sub> | F          | -30.91     | -8.0       | 7.0        |         |              |
|                  | Cd         | 13.8       |            |            |         |              |
| CdF <sub>2</sub> | F          | 44.35      |            |            |         |              |

TABLE III. Conduction-band offsets and Schottky barrier heights of interfaces studied in this work in electron volts.

| Interface                           | Experiment   | Models     |                                     |
|-------------------------------------|--|------------|-------------------------------------|
|                                     |  | This paper | Previous                            |
| Si/CaF <sub>2</sub>                 | 2.3 <sup>a</sup> , 2.2 <sup>b</sup> , 2.4 <sup>c</sup> | 2.2        |                                     |
| CaF <sub>2</sub> /CdF <sub>2</sub>  | 2.9 <sup>a</sup>                                       | 2.9        |                                     |
| Si/CoSi <sub>2</sub>                | 0.66 <sup>d,e</sup>                                    | 0.66       |                                     |
| CaF <sub>2</sub> /CoSi <sub>2</sub> |  | 3.0        | 2.0 <sup>f</sup> , 8.6 <sup>g</sup> |

<sup>a</sup>Reference 2.

<sup>b</sup>Reference 46.

<sup>c</sup>Reference 47.

<sup>d</sup>Reference 48.

<sup>e</sup>Reference 49.

<sup>f</sup>Reference 40.

<sup>g</sup>Reference 26.

sistent with one another. The Schottky barrier height (SBH) between Si and CoSi<sub>2</sub> is also well established. Since we are not aware of experiments for CoSi<sub>2</sub>/CaF<sub>2</sub>, we have combined the known Si/CoSi<sub>2</sub> SBH and the CaF<sub>2</sub>/Si conduction-band offset, assuming that these are values are transitive. The resulting 3.0 eV offset is somewhat higher than a previous estimate<sup>40</sup> of 2 eV, which was based on bulk work functions and electron affinities but much smaller than the huge offset of 8.6 eV predicted by recent linear augmented plane-wave calculations.<sup>26</sup> This large value is caused by the assumption that the difference between the experimental energy gap and the theoretical value of 7.8 eV within the local-density approximation (LDA) can be accounted for by a rigid upward shift of the conduction-band edge by 4.3 eV. However, previous calculations beyond LDA have shown that the error of LDA lies mostly in the valence-band edge that gets shifted downwards.<sup>41–43</sup> If one corrects the LDA results of Ref. 26 in this way, one obtains a Schottky barrier height that is close to our value given above.

#### IV. RESULTS AND DISCUSSION: RESONANT-TUNNELING STRUCTURES ON CoSi<sub>2</sub>-BASIS

In this section, we present studies of double- and triple-barrier tunneling diodes consisting of CoSi<sub>2</sub> quantum well layers and CaF<sub>2</sub> barriers. Since CoSi<sub>2</sub> is metallic and has a complex Fermi energy, it is far from obvious whether the electronic structure supports momentum and energy-conserving tunneling processes and it is even less clear whether the current-voltage characteristics exhibits sharp resonances. Concretely, we first consider a double-barrier tunneling diode, consisting of a 1.9 nm (= 6 triple layers) CoSi<sub>2</sub> quantum well in between two 1.2 nm (= 4 triple layers) CaF<sub>2</sub> barriers. A CoSi<sub>2</sub> cap layer on the top and an *n*-doped Si(111)-substrate serve as contacts. In the inset of Fig. 1, we show a schematic picture of the band profile of this structure, whereas the main part of the figure depicts the calculated current-voltage characteristics. Under forward bias, the metallic emitter on the left-hand side provides electrons at nearly all lateral wave vectors  $\mathbf{k}_{\parallel}$  below the Fermi energy. The doped Si on the right-hand side, on the other hand, accepts electrons only for wave vectors near the conduction-band minimum at  $\Delta$  and consequently acts as a momentum filter for low bias. Nevertheless, the calculated current reflects a high density of open channels that shows

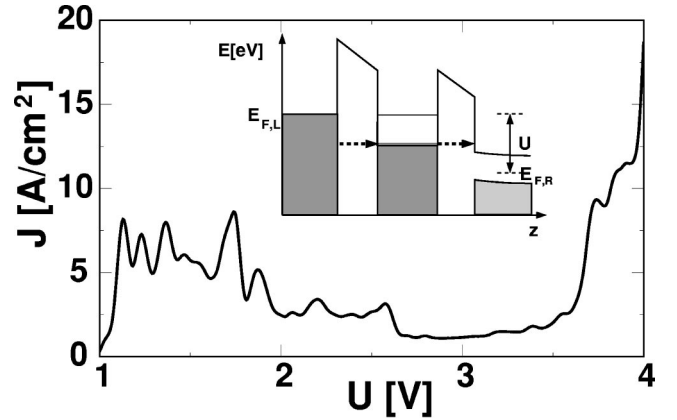


FIG. 1. Current-voltage characteristics of the double barrier CoSi<sub>2</sub>/CaF<sub>2</sub> resonant tunneling diode. The CoSi<sub>2</sub> well and the CaF<sub>2</sub> barriers consist of 6 and 4 triple layers, respectively. The inset indicates the band lineup for an applied bias  $U$  in volts schematically. Dark- and light-shaded areas represent occupied states in CoSi<sub>2</sub> and the valence band of the silicon substrate, respectively. The dashed arrows show a resonant-tunneling path through a quasi-bound state (horizontal lines).

that the metallic quantum well supplies a quasicontinuum of energy- and momentum-conserving tunneling states. The current shows some negative differential resistance effects but no distinct resonances.

The situation is very different for resonant triple-barrier CoSi<sub>2</sub>/CaF<sub>2</sub> resonant-tunneling diodes. In accordance with experimentally fabricated structures<sup>5,44</sup> we have theoretically analyzed a structure with a barrier thickness of 0.9 nm (3 triple layers), and well widths of 6 and 9 triple layers for the first and second CoSi<sub>2</sub> well, respectively. For an applied bias of 3.6 V, the corresponding band-edge energies are depicted in Fig. 2. Figure 3 compares the present theory for the current/voltage characteristics with the experimental data.<sup>44,5</sup> Strikingly, we find this tunneling diode to produce a very distinct resonance near 3.6 V in good agreement with experiment. Even the magnitude of the current density is in fair

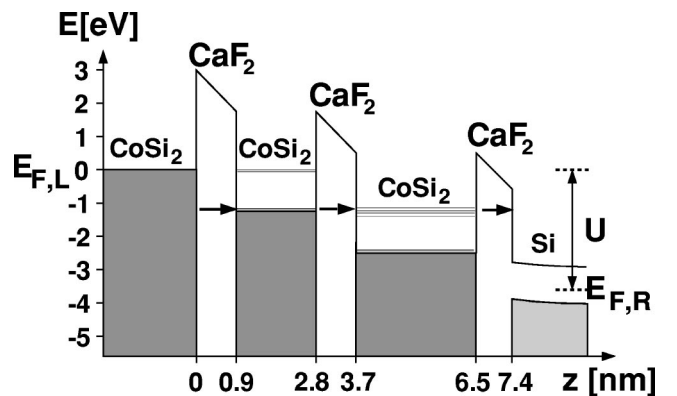


FIG. 2. Band-edge diagram of the triple barrier CoSi<sub>2</sub>/CaF<sub>2</sub> resonant-tunneling diode for an applied bias  $U$  of 3.6 V. The thickness of the layers is indicated on the abscissa in nm. Dark- and light-shaded areas represent occupied states in CoSi<sub>2</sub> and the valence band of the silicon substrate, respectively. The dashed arrows indicate schematically a resonant-tunneling path through two quasi-bound states indicated by horizontal lines at this particular voltage.

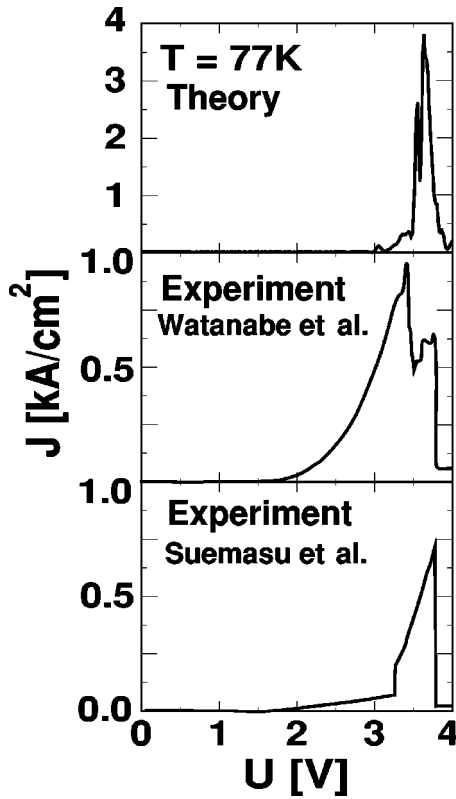


FIG. 3. Calculated (top) and measured (Refs. 44 and 5) (lower two plots) current-voltage characteristics of the triple barrier  $(\text{CaF}_2)_3/(\text{CoSi}_2)_6/(\text{CaF}_2)_3/(\text{CoSi}_2)_9/(\text{CaF}_2)_3$  heterostructure. The temperature is 77 K in all three cases.

accordance with the experimental data, taking into account the fact that any tunneling current depends exponentially on the barrier width and height.<sup>45</sup> Our calculations predict a peak-to-valley ratio for the current of about 32 for the structure in Fig. 3. Experimentally,<sup>5</sup> this ratio varies from sample to sample and shows a maximum ratio of 25 at liquid nitrogen temperature.

#### A. Origin of the resonance

In order to understand the origin of the very narrow resonance peak close to 3.6 V in the triple barrier structure (see Fig. 3), it is useful to consider the bulk  $\text{CoSi}_2$  band structure shown in Fig. 4(a) and the lateral dispersion of the electronic states in isolated  $\text{CoSi}_2$  quantum wells with 6 and 9 triple layers embedded in bulk  $\text{CaF}_2$ , as shown in Figs. 4(b) and 4(c). The bulk band structure exhibits several peaks in the density-of-states and we have marked one in particular by a circle in the band structure of Fig. 4(a) that has a predominantly Co- $d$  character. States of similar character in the two-dimensional density-of-states of the 9-layer  $\text{CoSi}_2$  quantum well are depicted in Fig. 4(c). These states possess a very small lateral dispersion and therefore give rise to a narrow tunneling resonance at 1.3 eV above the Fermi energy. This resonance is indicated schematically by a horizontal line in the band-edge diagram of Fig. 2. In addition, the present calculations reveal that the pseudomorphic interface leads to localized interface states that also have predominantly Co- $d$  character and possess a very small lateral dispersion for large  $k_{\parallel}$ . These states have an energy of roughly 50 to 100 meV

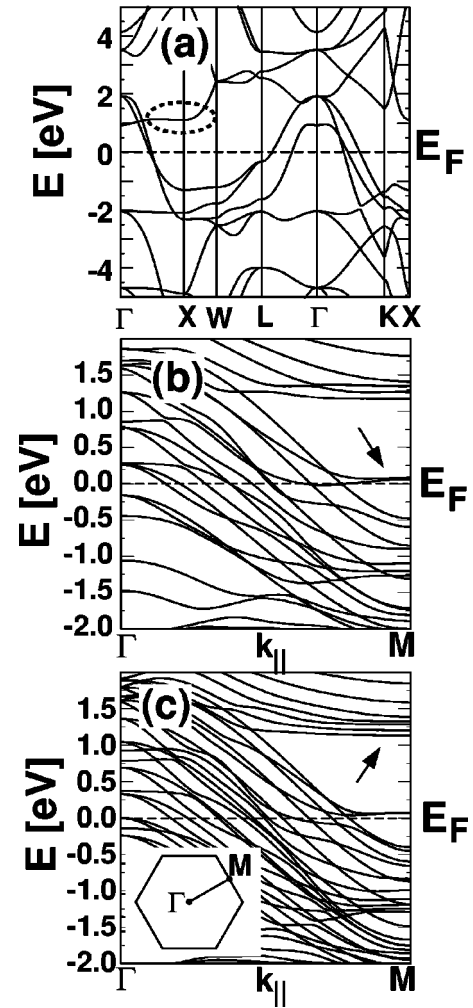


FIG. 4. (a) The calculated bulk band structure of  $\text{CoSi}_2$  in the  $sp^3d^5s^*$ -tight-binding model. (b) and (c) show the lateral energy-band dispersion from  $\Gamma \rightarrow M$  for  $\text{CoSi}_2$  quantum wells that are embedded into bulk  $\text{CaF}_2$  and consist of 6 and 9 atomic triple layers, respectively. The zero of energy is the Fermi level. The dotted circle and the arrows indicate flat bands that give rise to pronounced resonant tunneling peaks.

above the Fermi level and are marked with an arrow in Fig. 4(b). These states are sufficiently localized so that their energies do not change in broader quantum wells. These states are also depicted as horizontal lines in Fig. 2.

In the resonant-tunneling structure, the interface states in the first (leftmost) quantum well become aligned with the bulk resonance in the second quantum well at a bias of 3.6 V. In total, the spatially localized character of the  $d$ -states in  $\text{CoSi}_2$  cause the 2 metallic quantum wells to behave analogously to semiconductors with two quasibound states that are separated energetically by  $\sim 1.2$  eV. An important difference is that these states, originating in localized  $d$ -states rather than extended  $sp$ -like states, only weakly depend on the well width. Close inspection of all of these band structures shows that there are many more peaks in the density-of-states that, however, do not become mapped onto each other in energy and  $\mathbf{k}$  space in the tunneling structure. To illustrate this, Fig. 5 shows the transmission coefficient as a function of  $k_{\parallel}$  for the resonance bias and energy. They lead to countless small resonances that lead to the moderate peak

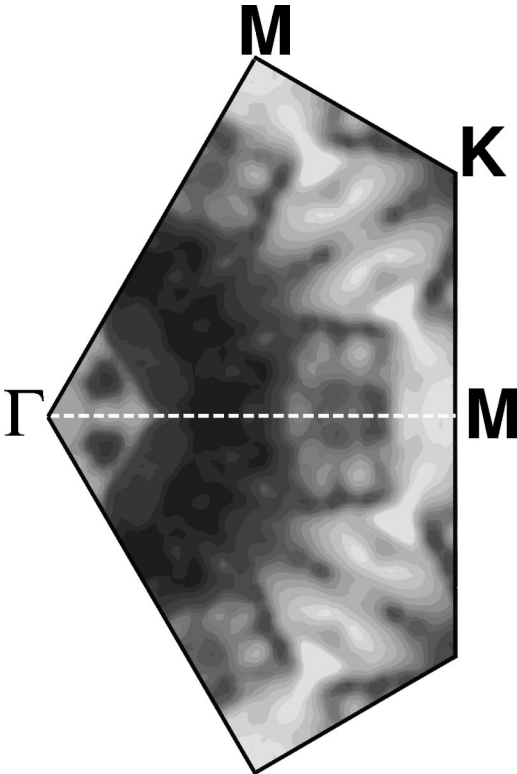


FIG. 5. The calculated transmission coefficient of the  $\text{CoSi}_2/\text{CaF}_2$  heterostructure depicted in Fig. 2 as a function of the lateral wave vector  $\mathbf{k}_\parallel$  for the resonance bias ( $U=3.6$  V) and the energy of  $-1.3$  eV below the left Fermi energy. The pattern reflects the  $C_{6V}$  symmetry in the  $[111]$  direction. White and dark areas correspond to high- and low-transmission coefficients on a logarithmic scale, respectively.

to valley ratio in the  $I$ - $V$  characteristics (Fig. 3) in spite of the fact that the present calculations only take into account the ballistic current.

### B. Stability of the resonance

Since a fluctuation of at least half a triple layer is unavoidable experimentally, it is essential to know whether the predicted resonances may actually get smeared out by growth related variations of the tunneling structure.

In addition, we can mimic part of the temperature effects by using a Fermi-Dirac distribution function at elevated temperatures. We note, however, that inelastic-scattering effects are neglected in the scattering formalism employed here. It turns out that these temperature effects do not significantly alter the results due to the high-barrier energy that amounts to more than 100 kT at room temperature. Our comparisons with experiment have therefore been consistently calculated with a Fermi distribution function for 77 K.

By changing the width of one of the metallic quantum wells, one alters the folding of the bulk band structure into the quantum well. Fortunately, our calculations show that a small variation of the well thickness by one or two triple layers (TL) (each 0.31 nm thick) does not shift the position of the resonance significantly. Figure 6 depicts the  $I$ - $V$  characteristics of triple barrier resonant-tunneling diodes (cf. Fig. 2) where the well widths of the first and second quantum

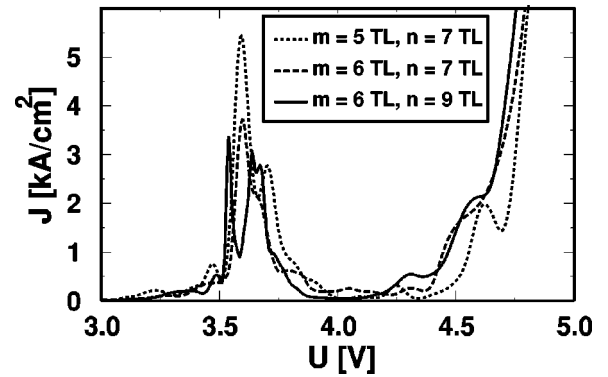


FIG. 6. Calculated current-voltage characteristics of the  $\text{CoSi}_2/\text{CaF}_2$  heterostructure depicted in Fig. 2 for different widths of the first (labeled by  $m$ ) and the second quantum well (labeled by  $n$ ), where the width is given in multiples of triple layers of  $\text{CoSi}_2$  (TL).

well have been varied between  $m=4 \dots 6$  TL and  $n=7 \dots 9$  TL, respectively. This stability is a consequence of the localized nature of the  $d$ -states discussed before. Thus, fluctuations of roughly one TL in the metallic layers do not affect the functioning of the device adversely.

If we change the width of the central barrier, on the other hand, we alter the relative voltage drops in all barriers and therefore shift the main resonance. In particular, a thicker central barrier shifts the current peak to a lower voltage. A thinner barrier, on the other hand, enhances the tunneling rate, broadens the resonances due to stronger wave function overlap, and therefore tends to smear out the peak in the  $I$ - $V$  characteristics. In Fig. 7, we show the effect of a thickness variation of the central  $\text{CaF}_2$  barrier. When this barrier is reduced to two triple layers, the  $I$ - $V$  curve has very little structure and practically no negative differential resistance. A central barrier that consists of 4 triple layers, on the other hand, shows a pronounced resonance near 3.0 V. This value is consistent with the assumption that the electric field is evenly distributed over the three barriers in the structure.

### V. RESULTS: RESONANT-TUNNELING STRUCTURES ON $\text{CdF}_2$ BASIS

The second class of tunneling structures that we have analyzed theoretically involve  $\text{CdF}_2/\text{CaF}_2$  heterostructures that

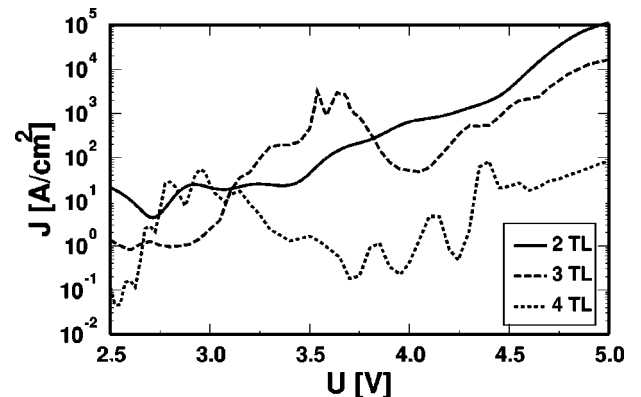


FIG. 7. Calculated current-voltage characteristics of  $\text{CoSi}_2/\text{CaF}_2$  heterostructure as shown in Fig. 2 for central barrier thicknesses of 2, 3 and 4  $\text{CaF}_2$  triple layers, respectively.

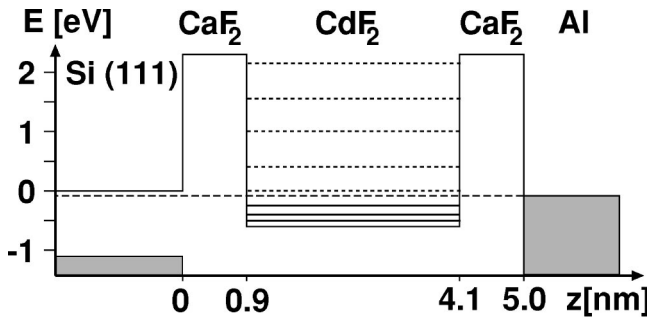


FIG. 8. Band-edge diagram of an unbiased  $\text{CdF}_2/\text{CaF}_2$  heterostructure. The electrons tunnel from the  $n$ -doped Si substrate on the left to the aluminum contact on the right. The thickness of the layers is indicated on the abscissa in nm. The full (dotted) lines in the  $\text{CdF}_2$ -quantum wells indicate calculated (quasi-) bound states. The dashed line indicates the Fermi level.

have also been fabricated and studied experimentally before.<sup>6,7</sup> These experiments used pseudomorphically grown layers of  $\text{CdF}_2$  and  $\text{CaF}_2$  on a highly  $n$ -doped Si(111) substrate with top aluminum contacts. The compounds  $\text{CaF}_2$  and  $\text{CdF}_2$  are insulators with band gaps of approximately 12 eV and 8 eV, respectively. Since the conduction-band edge of  $\text{CdF}_2$  lies approximately 2.9 eV below that of  $\text{CaF}_2$ , the former acts as a “quantum well” in this structure. The conduction band of  $\text{CdF}_2$  is dominated by a single,  $s$ -type parabolic band with its minimum at the  $\Gamma$  point<sup>39</sup> and an effective mass of 0.4 electron masses. The electronic band-edge structure of such a device is drawn in Fig. 8; there is a single  $\text{CdF}_2$  quantum well embedded in between  $\text{CaF}_2$  barriers. In the experiment, the substrate has been biased negatively against the metallic contact. Thus, in contrast to the  $\text{CoSi}_2$  case in the previous section, the electrons get injected from the  $n$ -doped Si. This implies that the emitted electrons originate from one of the six conduction-band minima along the  $\Delta$  axis. Since the Si substrate has [111] orientation, all 6 minima provide electrons with large  $k_{\parallel}$  values and will *not* be able to tunnel resonantly through the  $\text{CdF}_2$  well with its  $k_{\parallel}=(0,0)$  conduction-band minimum. The aluminum contact, on the other hand, has a Fermi surface that covers nearly the entire projected Brillouin zone and does not act as a momentum filter. Thus, altogether no negative differential resistance is expected for a  $\text{CdF}_2/\text{CaF}_2$  heterostructure when electrons are injected from an  $n$ -doped Si(111) substrate and this is indeed confirmed by a detailed calculation of the tunneling current. In Fig. 9, we show the calculated current-voltage characteristics of a  $(\text{CaF}_2)_3/(\text{CdF}_2)_{10}/(\text{CaF}_2)_3$  heterostructure with [111]-growth axis (solid line). As can be seen, this structure is highly resistive up to a bias of roughly 2.2 V.

The situation is completely different if one imagines an emitter that consists of  $n$ -Si but with a (001) orientation. In that case, two of the conduction-band minima that lie along the growth direction get projected onto the  $\Gamma$  point of the two-dimensional Brillouin zone. This opens a channel for momentum- and energy-conserving resonant tunneling through the quasibound states of the quantum well that also lie at the center of the Brillouin zone. The dashed  $I$ - $V$  characteristics represent the results for a heterostructure with

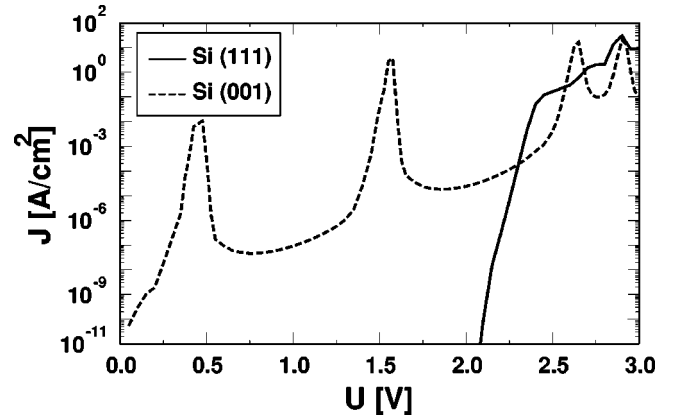


FIG. 9. Calculated current-voltage characteristics at 77 K of the planar  $\text{CdF}_2/\text{CaF}_2$  heterostructure depicted in Fig. 8 grown on a (111)-oriented (solid line) or (001)-oriented Si substrate (dashed line).

[001]-growth axis. These results indeed show distinct resonances in the current.

In contrast to these results, distinct current resonances and negative differential resistance has been observed even in some samples grown along the [111] direction.<sup>6</sup> In order to see how effective interface roughness can relax the momentum-selective resonant-tunneling process, we have repeated our tunneling current calculations for the (111) heterostructure, albeit with  $\text{CdF}_2/\text{CaF}_2$  interfaces with a “roughness” pattern that has been impressed onto them. For numerical reasons, we have modeled the roughness by a regular pattern that corresponds to a 4 by 1 lateral superlattice. The rim is 1 triple layer high and 1 primitive translation wide (along the  $[1\bar{1}0]$  direction) so that the momentum conservation gets reduced to multiples of a superlattice vector. This modification of the geometry has a dramatic impact on the current density (see Fig. 10) that now shows a distinct resonance close to where it appears experimentally. Still, the calculated current density is smaller than the experimental one. This is not surprising since we have broken the symme-

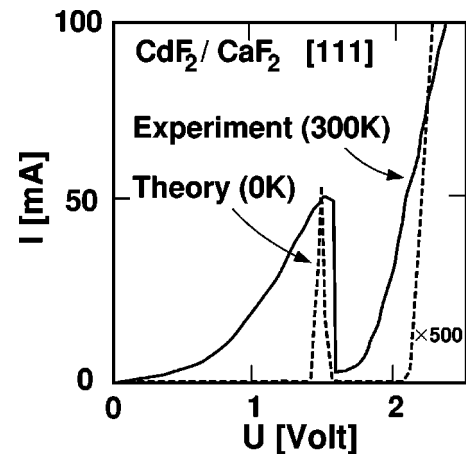


FIG. 10. Experimental (solid line) and theoretical (dashed line) current-voltage characteristics of the heterostructure shown in Fig. 8 with an impressed interface roughness corresponding to a single atomic triple layer, respectively. The temperatures are indicated in parentheses.

try rather artificially only along one direction.

Finally, we would like to point out that many more tunneling structures can be designed where momentum conservation does not restrict the tunneling process significantly. If one simply reverses the bias in the structure discussed above, for example, electrons get emitted from the aluminum contact and will have a broad spectrum of initial  $k_{\parallel}$  values. However, one then needs a second quantum well that acts as an energy selector.<sup>7</sup>

## VI. CONCLUSIONS

Employing an improved scattering scheme in the semi-empirical tight-binding framework, we calculated (coherent) current-voltage characteristics of various triple and double barrier RTD's on the basis of  $\text{CoSi}_2/\text{CaF}_2$  and  $\text{CdF}_2/\text{CaF}_2$  heterostructures. For the metal( $\text{CoSi}_2$ )/insulator( $\text{CaF}_2$ ) structure, we found in agreement with experiments a sharp resonance around 3.6 V bias, which is stable under moderate variations of the well thickness, but may be displaced by inhomogeneous barriers. The origin of the resonance could be traced back to the alignment of flat Co- $d$  bands of the

$\text{CoSi}_2$  quantum wells. At room temperature the peak-to-valley ratio of the coherent current decreases by a factor of 5 in comparison to  $T=0$  results.

As a result of  $k_{\parallel}$  conservation, the tunneling current of the double barrier  $\text{CdF}_2/\text{CaF}_2$ -heterostructure exhibits a strong dependence on the substrate orientation. For substrates with a (111) surface, negative differential resistance is predicted to occur only due to interface roughness, which was simulated by a lateral superlattice. The symmetry breaking induced by this imperfection, may account for the discrepancy between experimental data and calculations that assume flat interfaces. The same structure with an additional well and reversed bias shows theoretically as well as experimentally negative differential resistance at room temperature around 1.5 V.

## ACKNOWLEDGMENTS

The authors gratefully acknowledge fruitful discussions with J. A. Majewski, K. Hofmann, J. Wollschläger, and A. Klust. This work was supported by the Deutsche Forschungsgemeinschaft under Contract No. VO 483/4-1.

\*Electronic address: Strahberger@wsi.tum.de

†Electronic address: Vogl@wsi.tum.de

<sup>1</sup>A. Izumi, K. Tsutsui, and N.S. Sokolov, *Jpn. J. Appl. Phys.* **37**, 295 (1998).

<sup>2</sup>A. Izumi, Y. Hirai, K. Tsutsui, and N.S. Sokolov, *Appl. Phys. Lett.* **67**, 2792 (1995).

<sup>3</sup>L.J. Schowalter and R.W. Fathauer, *Science* **15**, 367 (1989).

<sup>4</sup>T. Suemasu, M. Watanabe, J. Suzuki, Y. Kohono, M. Asada, and N. Suzuki, *Jpn. J. Appl. Phys.* **33**, 57 (1994).

<sup>5</sup>T. Suemasu, M. Watanabe, M. Asada, and N. Suzuki, *Electron. Lett.* **28**, 1432 (1992).

<sup>6</sup>A. Izumi, N. Matsubara, Y. Kushida, K. Tsutsui, and N.S. Sokolov, *Jpn. J. Appl. Phys.* **36**, 1849 (1997).

<sup>7</sup>M. Watanabe, Y. Aoki, W. Saito, and M. Tsuganezawa, *Jpn. J. Appl. Phys.* **38**, L116 (1999).

<sup>8</sup>R. Tsu and L. Esaki, *Appl. Phys. Lett.* **22**, 562 (1973).

<sup>9</sup>K.V. Rousseau, K.L. Wang, and J.N. Schulman, *Appl. Phys. Lett.* **54**, 1341 (1989).

<sup>10</sup>D.H. Lee and J.D. Joannopoulos, *Phys. Rev. B* **23**, 4988 (1981).

<sup>11</sup>J.N. Schulman and Y.-C. Chang, *Phys. Rev. B* **27**, 2346 (1983).

<sup>12</sup>T.B. Boykin, J.P.A. van der Wagt, and J.S. Harris, Jr., *Phys. Rev. B* **43**, 4777 (1991).

<sup>13</sup>J.N. Schulman and D.Z.-Y. Ting, *Phys. Rev. B* **45**, 6282 (1992).

<sup>14</sup>D.Z.-Y. Ting, E.T. Yu, and T.C. McGill, *Phys. Rev. B* **45**, 3583 (1992).

<sup>15</sup>E.O. Kane, in *Tunneling Phenomena in Solids*, edited by E. Burstein and S. Lundqvist (Plenum, New York, 1969), p. 1.

<sup>16</sup>C. Strahberger and P. Vogl, *Physica B* **272**, 160 (1999).

<sup>17</sup>T.B. Boykin, *Phys. Rev. B* **54**, 7670 (1996).

<sup>18</sup>T.B. Boykin, *Phys. Rev. B* **54**, 8107 (1996).

<sup>19</sup>R.C. Bowen, W.R. Frensley, G. Klimbeck, and R.K. Lake, *Phys. Rev. B* **52**, 2754 (1995).

<sup>20</sup>R. Landauer, *IBM J. Res. Dev.* **32**, 306 (1988).

<sup>21</sup>M. Büttiker, *IBM J. Res. Dev.* **32**, 317 (1988).

<sup>22</sup>Aldo Di Carlo, P. Vogl, and W. Pötz, *Phys. Rev. B* **50**, 8358 (1994).

<sup>23</sup>W. A. Harrison, *Elementary Electronic Structure* (World Scientific, Singapore, 1999).

<sup>24</sup>J. Zegenhagen and J.R. Patel, *Phys. Rev. B* **41**, 5315 (1990).

<sup>25</sup>R.M. Tromp and M.C. Reuter, *Phys. Rev. Lett.* **61**, 1756 (1988).

<sup>26</sup>K. Akai and M. Matsuura, *Phys. Rev. B* **60**, 5561 (1999).

<sup>27</sup>J.M. Phillips and W.M. Augustyniak, *Appl. Phys. Lett.* **48**, 463 (1986).

<sup>28</sup>R.W. Fathauer, B.D. Hunt, and L.J. Schowalter, *Appl. Phys. Lett.* **49**, 64 (1986).

<sup>29</sup>N.S. Sokolov, N.N. Faleev, S.V. Gastev, N.L. Yakoviev, A. Izumi, and K. Tsutsui, *J. Vac. Sci. Technol. A* **13**, 2703 (1995).

<sup>30</sup>W.A. Harrison, *Phys. Rev. B* **24**, 5835 (1981).

<sup>31</sup>W.A. Harrison, *Phys. Rev. B* **28**, 550 (1983).

<sup>32</sup>P. Vogl, H.P. Hjalmarson, and J.D. Dow, *J. Phys. Chem. Solids* **44**, 365 (1983).

<sup>33</sup>M. Graf and P. Vogl, *Phys. Rev. B* **51**, 4940 (1995).

<sup>34</sup>S. Sanguinetti, C. Calegari, V.R. Velasco, G. Benedek, F. Tavazza, and Leo Miglio, *Phys. Rev. B* **54**, 9196 (1996).

<sup>35</sup>J.-M. Jancu, R. Scholz, F. Beltram, and F. Bassani, *Phys. Rev. B* **57**, 6493 (1998).

<sup>36</sup>D.A. Papaconstantopoulos, *Handbook of the Band Structure of Elemental Solids* (Plenum Press, New York, 1986).

<sup>37</sup>F. Gan, Y.-N. Xu, M.-Z. Huang, W.Y. Ching, and J.G. Harrison, *Phys. Rev. B* **45**, 8248 (1992).

<sup>38</sup>J. Barth, R.L. Johnson, and M. Cardona, *Phys. Rev. B* **41**, 3291 (1990).

<sup>39</sup>T. Mattila, S. Pöykkö, and R.M. Nieminen, *Phys. Rev. B* **56**, 15665 (1997).

<sup>40</sup>M. Asada, M. Watanabe, T. Suemasu, Y. Kohno, and W. Saitoh, *J. Vac. Sci. Technol. A* **13**, 623 (1995).

<sup>41</sup>M. Städele, M. Moukara, J.A. Majewski, P. Vogl, and A. Görling, *Phys. Rev. B* **59**, 10 031 (1999).

<sup>42</sup>Y. Hatsugai and T. Fujiwara, *Phys. Rev. B* **37**, 1280 (1988).

<sup>43</sup>A. Svane and O. Gunnarsson, *Phys. Rev. Lett.* **65**, 1148 (1990).

<sup>44</sup>M. Watanabe, T. Suemasu, S. Muratake, and M. Asada, *Appl. Phys. Lett.* **62**, 300 (1993).

<sup>45</sup>We note that the experimental current density has been extracted from Refs. 5 and 44 by dividing the measured current by the specified contact area.

<sup>46</sup>D. Rieger, F.J. Himpsel, U.O. Karlsson, F.R. McFeely, J.F. Morar, and J.A. Yarmoff, *Phys. Rev. B* **34**, 7295 (1986).

<sup>47</sup>P. Avouris and R. Wolkow, *Appl. Phys. Lett.* **55**, 1074 (1989).

<sup>48</sup>H. Sirringhaus, E.Y. Lee, U. Kafader, and H. von Känel, *J. Vac. Sci. Technol. B* **13** (4), 1848 (1995).

<sup>49</sup>T. Meyer and H. von Känel, *Phys. Rev. Lett.* **78**, 3133 (1997).